ACS OMEGA

http://pubs.acs.org/journal/acsodf

Article

Mesoscopic Inhomogeneities in Concentrated Electrolytes

Oksana Patsahan* and Alina Ciach

Cite This: *ACS Omega* 2022, 7, 6655−6664

Read Online

ACCESS | Metrics & More | Article Recommendations | Supporting Information

ABSTRACT: A mesoscopic theory for water-in-salt electrolytes combining density functional and field-theoretic methods is developed in order to explain the unexpectedly large period of the oscillatory decay of the disjoining pressure observed in recent experiments for the lithium bis(trifluoromethylsulfonyl)-imide (LiTFSI) salt [T. S. Groves et al., *J. Phys. Chem. Lett.* **2021**, *12*, 1702]. We assumed spherical ions with different diameters and implicit solvent, inducing strong, short-range attraction between ions of the same sign. For this highly simplified model, we calculated correlation functions. Our results indicate that mesoscopic inhomogeneities can occur when the sum of the Coulomb and the water-mediated interactions between like ions is attractive at short and repulsive at large distances. We adjusted the attractive part of the potential to the water-in-LiTFSI electrolyte and obtained both the period and the decay rate of the correlations, in semiquantitative agreement with the experiment. In particular, the decay length of the correlations increases nearly linearly with the volume fraction of ions.

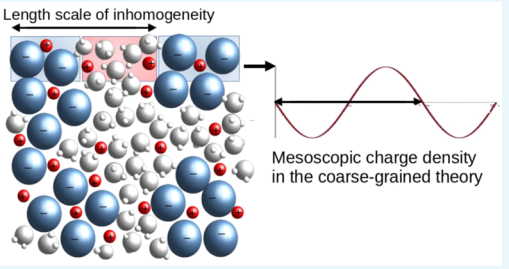

1. INTRODUCTION

For many years it was commonly assumed that dilute electrolytes, very well described by the Debye−Hückel (DH) theory, are more suitable for electrochemical devices than the concentrated ones. For this reason, neither experimentalists nor theoreticians paid much attention to the concentrated electrolytes. Recently, however, it was noted that the concentrated electrolytes have advantages such as a large electrochemical stability window, and they may find applications in electrochemical devices, for example, in lithium-ion batteries.[1−4] These observations motivated intensive experimental studies. On one hand, lithium salt/ionic liquid mixtures have been studied intensely because their unique properties of ionic liquids (IL) such as low volatility, low flammability, and high chemical and thermal stability make them attractive for technological applications as electrolytes. However, recent electrophoretic NMR measurements detected a negative alkali cation contribution to the total conductivity in a number of this type of mixture.[5,6] The experimental results were explained by the theory[7] and computer simulations.[8,9] On the other hand, water-in-salt electrolytes draw increasing attention as promising candidates for replacing current lithium-ion technology in state-of-the-art lithium-ion batteries.[1,2] It was found that when the concentration of ions, ρ, increases the deviation between experimental results and predictions of the DH theory becomes very large. Even qualitative trends well documented for the dilute electrolytes, such as decreasing screening length with increasing ρ, are opposite in concentrated electrolytes and IL solutions. Recent surface-force balance (SFB) experiments show that in the above systems the screening length λ_s is proportional to ρ, while the Debye screening length λ_D perfectly describing the dilute electrolytes is proportional to $1/\sqrt{\rho}$. The scaling behavior $\lambda_s/\lambda_D \sim (a/\lambda_D)^3$, where a is the average diameter of the ions, was found for a number of concentrated solutions of simple salts in water, IL solutions, and alkali halide solutions.[10−12] This universal behavior suggests that the observed decay of the disjoining pressure depends not on specific interactions but only on the Coulomb potential that is common for all the studied systems.

The strong disagreement of experimental results for concentrated electrolytes with DH theory predictions attracted the attention of theoreticians, but despite significant effort in theoretical and simulation studies, the experimental results are not fully explained yet.[13−22] In several theories and simulation studies, the scaling behavior $\lambda_s/\lambda_D \sim (a/\lambda_D)^\alpha$ was found, but the scaling exponent as well as λ_s in these studies were significantly smaller than in the experiments.[15−19,21,22] Correct scaling for the charge−charge correlation length (that should be equal to λ_s) was obtained in ref 23, where it was shown that the variance of the local charge density plays a significant role for large concentrations of ions. However, oscillatory decay obtained in theory is at variance with the asymptotic monotonic decay of the disjoining pressure observed in the experiments.[4,10−12]

Theoretical studies of ionic systems are very often based on the restricted primitive model (RPM) .[24,25] In the RPM, the

Received: October 27, 2021
Accepted: January 31, 2022
Published: February 16, 2022

© 2022 The Authors. Published by American Chemical Society

https://doi.org/10.1021/acsomega.1c06013
ACS Omega 2022, 7, 6655−6664

ions are treated as charged hard spheres with the same diameter, and the Coulomb potential between the ions is assumed. The solvent, however, is treated as a dielectric continuum. Theoretical results for the RPM[26−28] show that when the density of ions is very low and the temperature is very high the charge−charge correlations exhibit exponential decay with the decay length $\lambda_s = \lambda_D$, signaling that the ions behave as point charges and the DH theory is valid. For increasing ρ and/or decreasing T, however, the sizes of the ions become more and more important, and λ_s deviates more and more from λ_D. Moreover, a second exponential term with a decay length smaller than λ_s and an amplitude with opposite sign becomes relevant. The two decay lengths merge at the Kirkwood line[29] on the (ρ, T) diagram. At the large-density, low-temperature side of the Kirkwood line, the charge−charge correlation function exhibits an oscillatory decay with the period $\sim 2a$.[26,27] The neighborhood of opposite charges is more probable than the neighborhood of like charges, and at the Kirkwood line the density is large enough and the temperature is low enough to allow for formation of clusters with oppositely charged nearest neighbors, where the repeat unit is $2a$. The predictions concerning the period of the damped oscillations of the correlation function were verified by simulations and experiments.[11,12,22,30−32] The decay length of the correlations in the RPM, however, depends on the approximation used in theoretical studies and remains a question of a debate.[23,26,28]

For the charge density profile near a planar electrode, as well as for the disjoining pressure between parallel planar electrodes, the decay length and the period of oscillations are expected to be the same as the corresponding length in the charge−charge correlation function in the bulk electrolyte at the same thermodynamic state. In the SFB experiments, the oscillatory decay of the disjoining pressure was observed up to some distance between the crossed mica cylinders, but the asymptotic decay at larger distances was monotonic.[10−12]

Strong disagreement with the RPM predictions was observed in recent SFB experiments for concentrated lithium bis(trifluoromethylsulfonyl)-imide (LiTFSI) in water.[4] It was found that the period of oscillations of the disjoining pressure was twice as large as the sum of diameters of the cation and the anion, observed previously in many concentrated electrolytes and predicted by the RPM. The same length scale of inhomogeneities in the bulk was observed in scattering experiments for concentrated LiTFSI.[3] At large distances, the decay of the disjoining pressure changes from oscillatory to monotonic, as found before for the other systems. Importantly, the decay length increases with increasing salt concentration and is of the same order of magnitude as observed previously in various concentrated electrolytes.[4]

In the LiTFSI salt, the size and the chemical properties of the $TFSI^-$ and Li^+ ions are significantly different.[3] The $TFSI^-$ ion is not spherical and is much larger than the Li^+ ion. Moreover, the Li^+ ions are very well solvated in water, in contrast to the hydrophobic $TFSI^-$ ions. Based on the above observations, we conclude that in the above water-in-salt electrolyte the size difference between the ions and/or the specific non-Coulombic interactions must play a significant role and cannot be neglected.

The effect of specific interactions was studied in the RPM supplemented with additional short-range (SR) interactions in ref 33. On the other hand, the size difference between the ions with neglected SR (primitive model (PM)) was studied in refs 34−37. It was found that the length scale of inhomogeneities depended on the strength of the SR interactions and on the size asymmetry. These general predictions were not verified by experiments, however. In the particular case of LiTFSI, the question of the origin of the scale of inhomogeneities and of the range of correlations is open.

In this work, we develop a minimal model for the water-in-salt electrolyte and fit the parameters to the particular case of the LiTFSI salt. The minimal model can allow us to see which details of the system properties can be neglected without changing the key features of the decay of the correlations. The important questions are: (i) To what extent can properties of the systems with large size asymmetry of ions and with strong specific interactions depend on details of the interactions and on the geometry of the ions? (ii) Can the solvent be treated as a dielectric continuum that mediates effective ion−ion interactions, or must it be taken into account explicitly? (iii) What types of approximations should be used to compute the correlation functions reproducing the qualitative trends found in experiments?

In our model, we assume that both the size difference and the effective SR interactions between the ions must be taken into account. The solvent, however, can be treated as a dielectric continuum. We further assume that water induces effective ion−ion interactions of a range much shorter than the range of the Coulomb potential. The model is introduced in Section 2. In Section 3, we develop an approximate form of the grand thermodynamic potential functional of local ionic densities that allows us to obtain correlation functions. In Section 4, we calculate the correlation functions first in mean-field approximation (MF) (Section 4.1) and next beyond the MF, using the procedure developed in refs 38 and 39 (Section 4.2). We obtain a semiquantitative agreement with experiment when we assume strong water-induced, short-range attraction between the cations. The last section contains the discussion and summary.

2. CONSTRUCTION OF THE THEORETICAL MODEL

In this section, we describe the assumptions and the approximations leading to the effective specific interactions between the ions in the LiTFSI salt dissolved in water. We take into account the ionic sizes reported in ref 4. In addition, we develop the approximation for the SR interactions based on the requirement that the model predicts inhomogeneities at the length scale $\sim 2(\sigma_+ + \sigma_-) = 4a$, where $\sigma_\pm$ denotes the diameter of the corresponding ion. Once the form of the SR interactions is assumed, we calculate the correlation functions for different volume fractions of ions without further fitting of any parameters, using the method summarized in Section 3.

We first consider the excluded-volume interactions. The $TFSI^-$ ions are much bigger than the Li^+ ions and have a shape of an ellipsoid. We assume that the size difference is more important than the nonspherical shape and assume that the Li^+ and $TFSI^-$ ions can be modeled as charged hard spheres with the diameter $\sigma_+ = 0.2$ nm and $\sigma_- = 0.6$ nm, respectively.

From the previous studies,[3] we know that the Li^+ ions are strongly hydrophilic, while the $TFSI^-$ ions are strongly hydrophobic. The Li^+ ions are solvated by water, and the $TFSI^-$ ions are not. This means that the short-range non-Coulombic forces have a strong effect on the distribution of the ions and cannot be neglected. Even though the water−Li^+ interactions play an important role, we assume that water can be treated as a dielectric continuum, as in the PM and the

https://doi.org/10.1021/acsomega.1c06013
ACS Omega 2022, 7, 6655−6664

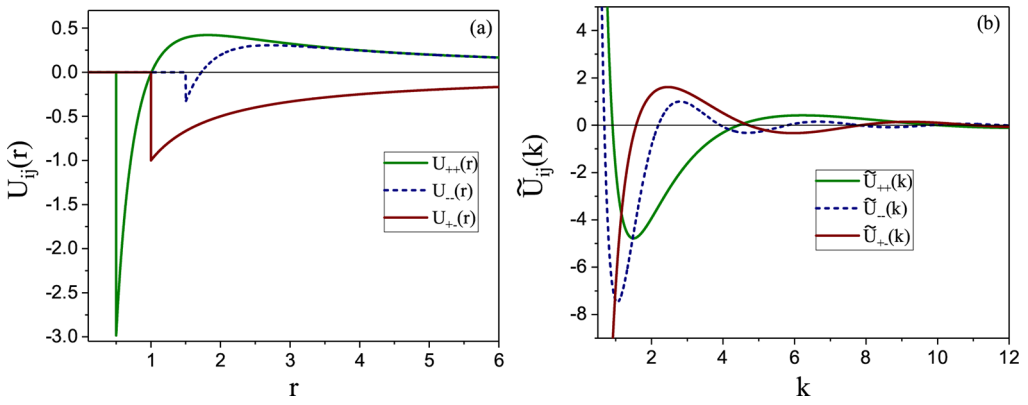

Figure 1. Interaction potentials $U_{ij}(r)$ (eqs 1−6) for the model with $\delta = 0.5$, $\epsilon^*_{++} = 5$, and $\epsilon^*_{--} = 1$ in real space (a) and in Fourier representation (b). U_{ij} are in units of E_C. E_C and δ are defined in eqs 5 and 7. r and k are in a and a^{-1} units, respectively, where $a = (\sigma_+ + \sigma_-)/2$.

classical DH theory. We assume, however, that water molecules mediate effective interactions between the Li^+ ions and that these solvent-induced effective interactions are short-ranged (compared to the Coulomb potential) but strong. In addition, we assume short-range interactions between the $TFSI^-$ ions but neglect the interactions between the Li^+ and $TFSI^-$ ions other than the Coulomb potential. We do not attempt to determine the precise shape of these interactions because the correlations at large distances depend only on some gross features of the potentials, such as their range and strength. This is because in collective phenomena involving many ions and solvent molecules many details are washed out by averaging over all distributions of the ions and the solvent molecules.

With the above assumptions, we model the aqueous electrolyte solution as a binary mixture of oppositely charged hard spheres of different diameters ($\sigma_+ \neq \sigma_-$) immersed in a structureless dielectric medium with the dielectric constant ε. We limit ourselves to the model with monovalent ions ($z_+ = z_- = 1$). The presence of the solvent is taken into account through the solvent-induced effective short-range attractive interactions between the ions of the same sign. Therefore, we assume that the pair interaction potentials between two ions for $r > \sigma_{\alpha\beta} = (\sigma_\alpha + \sigma_\beta)/2$, with $\alpha = +, -$ and $\beta = +, -$, can be presented in the form

$$U_{\alpha\beta}(r) = U^C_{\alpha\beta}(r) + U^A_{\alpha\beta}(r) \tag{1}$$

Here, $U^C_{\alpha\beta}(r)$ are the Coulomb potentials between the ions with the signs α and β. As a length unit we choose the sum of radii, $a = (\sigma_+ + \sigma_-)/2$. The Coulomb potentials for $r^* \equiv r/a$ are

$$\beta U^C_{++}(r^*) = \frac{l_B \theta(r^* - a_+)}{r^*} \tag{2}$$

$$\beta U^C_{--}(r^*) = \frac{l_B \theta(r^* - a_-)}{r^*} \tag{3}$$

$$\beta U^C_{+-}(r^*) = -\frac{l_B \theta(r^* - 1)}{r^*} \tag{4}$$

where $a_\pm = \sigma_\pm/a$

$$l_B = \frac{1}{T^*} = \beta E_C, \qquad E_C = \frac{e^2}{a\varepsilon} \tag{5}$$

and $\beta = 1/k_B T$ with k_B and T denoting the Boltzmann constant and temperature, respectively. l_B is the Bjerrum length in a units; E_C is the electrostatic potential of the pair of oppositely charged ions at contact; and the reduced temperature T^* is in units of E_C. The unit step function $\theta(x) = 1$ for $x > 0$ and $\theta(x) = 0$ for $x < 0$ prevents contributions to the electrostatic energy of the pair of ions that would come from the forbidden overlap of the hard cores.

For $U^A_{\alpha\alpha}(r)$, we assume a short-range attractive potential. The form of the sum of the direct (van der Waals type) and solvent-induced interactions is unknown, but we assume that its detailed shape is not necessary for studies of the collective phenomena such as the long-distance correlations. For simplicity of calculations, we assume the attractive Yukawa potentials for $U^A_{\alpha\alpha}(r)$

$$\beta U^A_{\alpha\alpha}(r^*) = -l_B \epsilon^*_{\alpha\alpha} a_\alpha \frac{e^{-z^*_\alpha (r^* - a_\alpha)}}{r^*} \theta(r^* - a_\alpha), \qquad \alpha = +, - \tag{6}$$

where z^*_α is in the a^{-1} units, and we assume that $z^*_+ = z^*_- = z = 1.8$ to ensure fast decay of these interactions. $\epsilon^*_{\alpha\alpha}$ measures the strength of the effective non-Coulombic interactions in units of E_C. Introducing the size-asymmetry parameter

$$\delta = \frac{\sigma_- - \sigma_+}{\sigma_- + \sigma_+} \tag{7}$$

we get $a_\pm = 1 \mp \delta$.

We assume that for the $TFSI^-$ ions $\epsilon^*_{--} = 1$ and treat ϵ^*_{++} as a fitting parameter. In order to find the best approximation for the Li^+ ions in water, we calculate the length scale of inhomogeneities for arbitrary ϵ^*_{++} in Section 4.1. We find that $\epsilon^*_{++} = 5$ leads to a satisfactory agreement of the length scale of inhomogeneities with the experimental results. Based on this observation, we assume $\epsilon^*_{++} = 5$ for the considered system. Note that the second important length scale, λ_s, will be determined for several concentrations of ions without additional fitting.

In Figure 1(a) the potentials $U_{\alpha\beta}(r)$ normalized by $E_C = e^2/(a\varepsilon)$ are shown for the model with $\epsilon^*_{++} = 5$, $\epsilon^*_{--} = 1$, and $\delta = 0.5$. For the chosen parameters, the interaction potentials between like ions consist of short-range attraction (SA) and electrostatic long-range repulsion (LR). Competing interaction potentials of this kind are also known as SALR potentials. In one-component systems, the SALR-type interactions can lead to spontaneously formed stable aggregates of particles, such as

https://doi.org/10.1021/acsomega.1c06013
ACS Omega 2022, 7, 6655−6664

spherical or elongated clusters, networks, or layers.[40−42] The Fourier transforms of the potentials $U_{\alpha\beta}(r)/E_c$ for the above-mentioned model are shown in Figure 1(b), and the corresponding expressions are given in the Supporting Information. It is seen that $\tilde{U}_{++}(k)$ and $\tilde{U}_{--}(k)$ take minima at $k \neq 0$ which are rather close to each other. $\tilde{U}_{\alpha\alpha}(k) < 0$ means that the density wave of the α ions with the wavelength $2\pi/k$ leads to the energy lower than in the homogeneous state, signaling a high probability of such waves.

3. THEORETICAL FORMALISM: A BRIEF SUMMARY

In this section, we present a brief description of the mesoscopic theory for inhomogeneous mixtures.[38,43] In this theory, we divide the system into subsystems having mesoscopic sizes and consider the local volume fraction of the anions and the cations in each subsystem. Thus, our approach with the focus on each mesoscopic part of the system and its state differs from the approach with the focus on the ions and their states. The linear size of the mesoscopic subsystems should not be larger than the scale of the inhomogeneities. The local volume fraction of the ions with the α sign in the mesoscopic subsystem with the center at $\mathbf{r}$ is denoted by $\zeta_\alpha(\mathbf{r})$. By analogy with the macroscopic volume fraction, $\zeta_\alpha(\mathbf{r})$ denotes the fraction of the volume of the mesoscopic region that is occupied by the α-sign ions. For a given macroscopic volume fraction, there are plenty of microscopic states with different positions of the ions. Likewise, for the given $\zeta_\alpha(\mathbf{r})$, the positions of the ions can be different. The functions $\zeta_\alpha(\mathbf{r})$ can be considered as constraints imposed on the microscopic states. This constraint imposed on a particular subsystem at $\mathbf{r}$ is analogous to the constraint of a fixed number of ions in the whole system in the canonical ensemble. The canonical and grand canonical ensembles are equivalent in the thermodynamic limit because the variance of the number of ions, $\sigma_N = \langle N_\alpha^2\rangle - \langle N_\alpha\rangle^2$, is proportional to N_α, and $\sqrt{\sigma_N}/N_\alpha \propto 1/\sqrt{N_\alpha} \to 0$ for $N_\alpha \to \infty$. When mesoscopic inhomogeneities spontaneously appear in the fluid phase, however, the fluctuations of the local volume fraction, i.e., the local deviations of the volume fraction from its average value $\overline{\zeta}_\alpha$, cannot be neglected. The local volume fraction is larger or smaller than $\overline{\zeta}_\alpha$ when the cluster enters or leaves the considered region, and the states with $\zeta_\alpha(\mathbf{r})$ larger or smaller than $\overline{\zeta}_\alpha$ give more important contributions to the grand potential of the whole system as inhomogeneity gets stronger. The strength of the inhomogeneity can be measured by the variance $\langle(\zeta_\alpha(\mathbf{r}) - \overline{\zeta}_\alpha)^2\rangle$ of the local volume fraction. The linear extent of the inhomogeneity is determined by the wavelength of the density waves that gives the largest decrease of the system energy compared to the homogeneous state and depends on the interaction potentials.

Let us first consider our system with a particular distribution of the local volume fractions and with frozen fluctuations. Such a system for a given $\zeta_\alpha(\mathbf{r})$ represents a set of subsystems such that the exchange of the ions between different subsystems is forbidden, and the grand potential is $\Omega_{co} = -k_BT \ln \Xi_{co}$, with Ξ_{co} denoting the summation of $\exp(-\beta H)$, where H is the microscopic Hamiltonian, over the microscopic states compatible with $\zeta_\alpha(\mathbf{r})$. Because of the frozen mesoscopic fluctuations, our "locally canonical" ensemble can be reasonably well described within the MF approximation.

The grand thermodynamic potential in the presence of the above mesoscopic constraints (frozen mesoscopic fluctuations) can be written in the form

$$\Omega_{co}[\zeta_+, \zeta_-] = U_{co}[\zeta_+, \zeta_-] - TS[\zeta_+, \zeta_-] - \mu_\alpha \int d\mathbf{r}\zeta_\alpha(\mathbf{r})$$

where U_{co}, S, and μ_α are the internal energy, the entropy, and the chemical potential of the species α, respectively. Hereafter, the summation convention for repeated indices is used. We make the approximation $-TS = \int d\mathbf{r} f_h(\zeta_+(\mathbf{r}), \zeta_-(\mathbf{r}))$, where $f_h(\zeta_+(\mathbf{r}), \zeta_-(\mathbf{r}))$ is the free-energy density of the hard-core reference system in the local-density approximation

$$\beta f_h = \rho_+ \ln \rho_+ + \rho_- \ln \rho_- + \beta f_{hs}$$

where the first two terms come from the entropy of mixing, and f_{hs} is the contribution to the free energy density associated with packing of hard spheres with two different diameters. The expression for f_{hs} in the Carnahan−Starling approximation[44] is given in the Supporting Information. Since we are interested in correlations between local fluctuations in regions separated by large distances, more accurate forms of the contribution to the entropy associated with packing of hard spheres, such as in ref 45, are an unnecessary complication.

In MF, the internal energy U_{co} is given by the expression

$$U_{co}[\zeta_+, \zeta_-] = \frac{1}{2}\int d\mathbf{r}_1 \int d\mathbf{r}_2 V_{\alpha\beta}(|\mathbf{r}_1 - \mathbf{r}_2|)\zeta_\alpha(\mathbf{r}_1)\zeta_\beta(\mathbf{r}_2)$$

Because $\zeta_\alpha = \pi\rho_\alpha\sigma_\alpha^3/6$ is used in the above definition, we have rescaled the interaction potential, $V_{\alpha\beta}(r) = U_{\alpha\beta}(r)/(\nu_\alpha\nu_\beta)$, where $\nu_\alpha = \pi\sigma_\alpha^3/6$.

When the constraints imposed on the microscopic states by $\overline{\zeta}_\alpha$ are released and the ions can move from one subsystem to the other, the microscopic states incompatible with $\overline{\zeta}_\alpha$ can appear. The average volume fractions can remain equal to $\overline{\zeta}_\alpha$ when the fluctuations $\Delta\zeta_\alpha(\mathbf{r}) = \zeta_\alpha(\mathbf{r}) - \overline{\zeta}_\alpha$ cancel one another, but the grand potential contains the fluctuation contribution and has the form[43]

$$\beta\Omega[\zeta_+, \zeta_-] = \beta\Omega_{co}[\zeta_+, \zeta_-] - \ln\left[\int D\Delta\zeta_+ \int D\Delta\zeta_- e^{-\beta H_{fluc}}\right] \quad (8)$$

In eq 8, $\int D\Delta\zeta_\alpha$ denotes the functional integral over the mesoscopic fluctuations $\Delta\zeta_\alpha$ that according to the Landau theory[46] appear with the probability proportional to the Boltzmann factor $\exp(-\beta H_{fluc})$, with

$$H_{fluc} = \Omega_{co}[\zeta_+ + \Delta\zeta_+, \zeta_- + \Delta\zeta_-] - \Omega_{co}[\zeta_+, \zeta_-]$$

denoting the change of Ω_{co} when the fluctuation $\Delta\zeta_\alpha$ appears. Thus, in our theory the contributions to the grand potential from the microscopic and the mesoscopic degrees of freedom are given in the first and second terms in eq 8, respectively. In MF, i.e., with frozen mesoscopic fluctuations, the second term on the RHS of eq 8 is neglected.

We are interested in the correlation functions in the disordered phase

$$G_{\alpha\beta}(\mathbf{r}) = \langle\Delta\zeta_\alpha(\mathbf{r}_0)\Delta\zeta_\beta(\mathbf{r} + \mathbf{r}_0)\rangle, \quad \alpha, \beta = +, - \quad (9)$$

where the averaging is with the probability proportional to $\exp(-\beta H_{fluc})$. The matrix $\mathbf{G}$ with the elements defined in eq 9 satisfies the analogue of the Ornstein−Zernike equation, $\mathbf{G} = \mathbf{C}^{-1}$, where the inverse correlation functions $\tilde{C}_{\alpha\beta}$ are the second functional derivatives of $\beta\Omega[\zeta_+, \zeta_-]$ with respect to ζ_α and ζ_β.[43] In the lowest-order nontrivial approximation beyond MF[38,43]

https://doi.org/10.1021/acsomega.1c06013
ACS Omega 2022, 7, 6655−6664

$$\tilde{C}_{\alpha\beta}(k) = \beta\tilde{V}_{\alpha\beta}(k) + A_{\alpha\beta} + \frac{A_{\alpha\beta\gamma\delta}}{2}\mathcal{G}_{\gamma\delta} \tag{10}$$

where $\tilde{f}(k)$ denotes the function f in Fourier representation. In the above equation

$$A_{\alpha_1 \ldots \alpha_j} = \frac{\partial^j \beta f_h(\zeta_+, \zeta_-)}{\partial\zeta_{\alpha_1} \ldots \partial\zeta_{\alpha_j}} \tag{11}$$

with $\alpha_i = +, -$. Note that in this approximation the dependence of $\tilde{C}_{\alpha\beta}(k)$ on k comes only from $\beta\tilde{V}_{\alpha\beta}(k)$. The last term in eq 10 is the fluctuation contribution and comes from the last term in eq 8. In the Brazovskii-type approximation[47]

$$\mathcal{G}_{\gamma\delta} = \langle \Delta\zeta_\gamma(\mathbf{r})\Delta\zeta_\delta(\mathbf{r})\rangle = \int \frac{d\mathbf{k}}{(2\pi)^3}\tilde{G}_{\gamma\delta}(k) \tag{12}$$

Note that $\mathcal{G}_{\alpha\alpha} = \langle \Delta\zeta_\alpha(\mathbf{r})\Delta\zeta_\alpha(\mathbf{r})\rangle$ is the local variance of ζ_α; i.e., $\sqrt{\mathcal{G}_{\alpha\alpha}}$ is the standard deviation from the space-averaged value of the local volume fraction of the α-ions. The larger $\mathcal{G}_{\alpha\alpha}$ is, the stronger the mesoscopic inhomogeneity and the less accurate the MF approximation. Equations 10−12 have to be solved self-consistently. In general, it is a nontrivial task.

We focus on the disordered inhomogeneous phase and assume that the inhomogeneity occurs on a well-defined length scale corresponding to the largest decrease of the energy and is quite strong, as in the case of ref 4. Because of this assumption, our considerations from now on are limited to the thermodynamic states where strong inhomogeneity at well-defined length scales is present. For weaker inhomogeneity, the set of the integrals, eqs 10−12, and $\mathbf{G} = \mathbf{C}^{-1}$ must be solved. In our case, the peak of $\tilde{G}_{\gamma\delta}(k)$ (proportional to the structure factor) is high and narrow. For functions with a high, narrow peak, the main contribution to the integral comes from the vicinity of the maximum. We assume that the maximum of all the integrands in eq 12 is very close to the minimum at $k = k_0$ of $\det \tilde{\mathbf{C}}(k)$, and we make the approximation

$$\mathcal{G}_{\alpha\beta} = [\tilde{C}_{\alpha\beta}(k_0)]\mathcal{G} \tag{13}$$

where $[\tilde{C}_{\alpha\alpha}(k)] = \tilde{C}_{\beta\beta}(k)$ and $[\tilde{C}_{\alpha\beta}(k)] = -\tilde{C}_{\alpha\beta}(k)$ for $\alpha \neq \beta$ and

$$\mathcal{G} = \int \frac{d\mathbf{k}}{(2\pi)^3}\frac{1}{\det \tilde{\mathbf{C}}(k)} \tag{14}$$

Near the minimum at k_0, we have the approximation

$$\det \tilde{\mathbf{C}}(k) = D_0 + \frac{\beta\tilde{W}''(k_0)}{2}(k - k_0)^2 + \ldots \tag{15}$$

where $D_0 = \det \tilde{\mathbf{C}}(k_0)$ and $\beta W''(k_0)$ is the second-order derivative of $\det \tilde{\mathbf{C}}(k)$ with respect to the wavenumber k at $k = k_0$. From the approximations 15 and 14, we obtain[43,48]

$$\mathcal{G} \approx \frac{k_0^2}{\pi\sqrt{2\beta\tilde{W}''(k_0)D_0}}$$

With all the above assumptions, the problem reduces to determination of the minimum of $\det \tilde{\mathbf{C}}(k)$ and to a solution of three algebraic equations for $\tilde{C}_{\alpha\beta}(k_0)$ (see eqs 10 and 13) because

$$\tilde{C}_{\alpha\beta}(k) = \tilde{C}_{\alpha\beta}(k_0) + \beta\Delta\tilde{V}_{\alpha\beta}(k), \quad \alpha, \beta = +, - \tag{16}$$

where

$$\Delta\tilde{V}_{\alpha\beta}(k) = \tilde{V}_{\alpha\beta}(k) - \tilde{V}_{\alpha\beta}(k_0) \approx \frac{V''_{\alpha\beta}(k_0)}{8k_0^2}(k^2 - k_0^2)^2 \tag{17}$$

The last approximation is valid for $k \approx k_0$.

It should be noted that the results obtained within the framework of this theory for several models of inhomogeneous mixtures were verified by simulations.[38,39,49]

4. RESULTS

4.1. MF Approximation. In MF, we neglect the last term in eq 10 and easily obtain explicit expressions for the matrix $\tilde{\mathbf{C}}^{\mathrm{MF}}(k)$ inverse to the matrix of correlations. These expressions are shown in the Supporting Information. In MF, the disordered phase becomes unstable with respect to oscillatory modulations of the volume fractions of the ions at the so-called λ-line on the $(\bar{\zeta},T^*)$ diagram. The λ-line marks the boundary of stability of the disordered phase with respect to mesoscopic fluctuations of the volume fractions and separates the phase space into regions corresponding to the homogeneous and inhomogeneous (on the mesoscopic length scale) phases. Thus, in MF the λ-line is interpreted as a continuous order−disorder transition. In order to get the λ-line, one should solve the system of equations

$$\det \tilde{\mathbf{C}}^{\mathrm{MF}}(k_0) = 0,$$
$$\left.\frac{d \det \tilde{\mathbf{C}}^{\mathrm{MF}}}{dk}\right|_{k=k_0} = 0 \tag{18}$$

When the λ-line is crossed, the inhomogeneities in the distribution of ions occur on the length scale $2\pi/k_0$. In our model, k_0 depends in particular on ϵ^*_{++} that we left as a free parameter. In order to fit ϵ^*_{++} to our water-in-salt system, we need to have $2\pi/k_0 \approx 4$ in a units ($k_0 \approx 1.6$ in a^{-1} units), for the molarity $M \sim 3$−5 for which the experimental data were obtained. The volume fraction of the spherical ions with $\sigma_+ = 0.2$ nm and $\sigma_- = 0.6$ nm is related to the molarity M by $\bar{\zeta}/M = \frac{\pi}{6}(0.2^3 + 0.6^3)10^{-24}N_A$, where N_A is the Avogadro number. We get $\bar{\zeta} \approx 0.27$ and $\bar{\zeta} \approx 0.32$ for the 3.8 M and 4.6 M systems, respectively. However, the above formula is a very rough estimation for $\bar{\zeta}/M$ in view of the strong dependence of $\bar{\zeta}$ on the diameter of the ions and the ellipsoidal shape of the $TFSI^-$ anions, and it only gives the order of magnitude of M in the experimental system for the given $\bar{\zeta}$ in our theory. Thus, in our semiquantitative analysis, we will consider volume fractions up to $\bar{\zeta} = 0.55$.

The plot of k_0 as a function of ϵ^*_{++} for $\epsilon^*_{--} = 1$, $\delta = 0.5$, and $\bar{\zeta} = 0.45$ is shown in Figure 2. We can see that for $\epsilon^*_{++} = 5$ the length scale of inhomogeneities is $2\pi/k_0 \approx 3.9$ (in a-units), which for $a = 0.4$ nm gives 1.56 nm, which is close to the experimental result of 1.4 nm. We thus choose $\epsilon^*_{++} = 5$ in our further calculations.

Figure 3 shows the λ-line in the $\bar{\zeta}$—T^* (panel a) and $\bar{\zeta}$—k_0 (panel b) coordinates for the model with $\delta = 0.5$, $\epsilon^*_{++} = 5$, and $\epsilon^*_{--} = 1$. For the thermodynamic states below the λ-line, the waves with the wavelength $2\pi/k_0$ are more probable than the constant volume fractions. For our model, the emergence of the inhomogeneous structure for $\det \tilde{\mathbf{C}}^{\mathrm{MF}}(k_0) < 0$ may be associated with the formation of aggregates such as clusters or layers, rather than with a phase transition. For such thermodynamic states, the fluctuations dominating on the

https://doi.org/10.1021/acsomega.1c06013
ACS Omega 2022, 7, 6655−6664

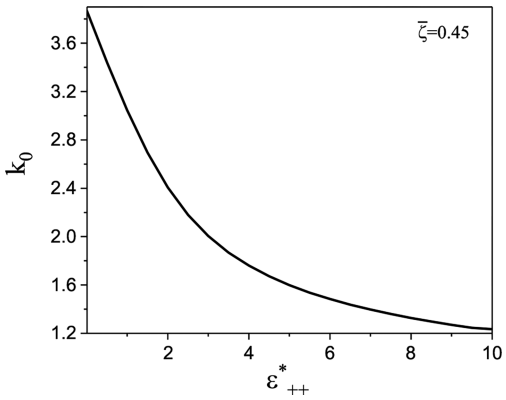

Figure 2. Wavenumber of the density waves k_0 (in a^{-1} units) as a function of ϵ^*_{++} for ϵ^*_{--}= 1, δ = 0.5, and the volume fraction of ions $\overline{\zeta}$ = 0.45. $\epsilon^*_{\alpha\alpha}$ describes the strength of the non-Coulombic interactions (see eq 6), and the size asymmetry δ is defined in eq 7. For the considered system, $a = (\sigma_+ + \sigma_-)/2 \approx 0.4nm$.

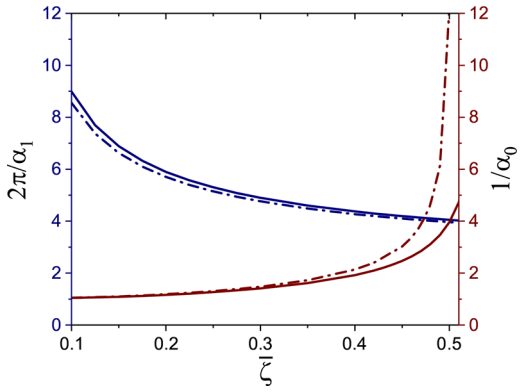

Figure 4. Model with δ = 0.5, ϵ^*_{++} = 5.0, and ϵ^*_{--} = 1.0. The decay length $\lambda_s = \alpha_0^{-1}$ and the period of oscillations $\lambda = 2\pi/\alpha_1$ of the correlation functions $G_{\alpha\beta}(r)$ as a function of the total volume fraction of ions $\overline{\zeta}$ for T^* = 1.5 (solid line) and T^* = 1.6 (dash-dotted line) in the MF approximation. α_0 and α_1 are in the a^{-1} units, with $a = (\sigma_+ + \sigma_-)/2 \approx 0.4$ nm.

mesoscopic length scale should be taken into account in order to restore the stability of the disordered phase. As found in different systems with spontaneously appearing mesoscopic inhomogeneities, fluctuations induce a change of the continuous transition found in MF to the first-order crystallization that is also shifted to higher volume fractions. Because of the instability of the disordered phase for $T^* < T^*_\lambda$ in MF, the asymptotic decay of the correlation functions $G^{MF}_{\alpha\beta}(r)$ can be analyzed only for $T^* > T^*_\lambda$.

In general, the long-range behavior ($r \gg 1$) of $G_{\alpha\beta}(r)$ is described by the function[50]

$$G_{\alpha\beta}(r) = \mathcal{A}_{\alpha\beta} e^{-\alpha_0 r} \sin(\alpha_1 r + \theta_{\alpha\beta})/r \quad (19)$$

In eq 19, $\alpha_0 = 1/\lambda_s$ and $\alpha_1 = 2\pi/\lambda$ are the imaginary and real parts of the leading order pole of $\tilde{G}_{\alpha\beta}(q)$ in the complex q-plane, which is determined as the complex root $q = i\alpha_0 \pm \alpha_1$ of the equation $\det \tilde{\mathbf{C}}(q) = 0$ having the smallest imaginary part. Since all $\tilde{G}_{\alpha\beta}(q)$ have a common denominator $\det \tilde{\mathbf{C}}(q)$, they exhibit the same pole structure and have the same exponential contributions. Only the amplitudes $\mathcal{A}_{\alpha\beta}$ and the phases $\theta_{\alpha\beta}$ differ for different $\alpha\beta$ combinations.

We calculate α_0 and α_1 for our model in MF from the equation $\det \tilde{\mathbf{C}}^{MF}(q) = 0$. The $\overline{\zeta}$-dependence of both the decay length $\lambda_s = \alpha_0^{-1}$ and the period of oscillations $\lambda = 2\pi/\alpha_1$ of the correlation functions $G_{\alpha\beta}(r)$ is presented in Figure 4 for two values of the reduced temperature, T^* = 1.5 and T^* = 1.6 ($T^* > T^*_\lambda$). Note that the decay length α_0^{-1} tends to ∞ ($\alpha_0 \to 0$), and simultaneously the period of oscillations λ tends to $2\pi/k_0 \approx 4a$ when $T^* \to T^*_\lambda$. More precisely, we get $\lambda = 3.96\ a$ for T^* = 1.5, $\overline{\zeta}$ = 0.5 and $\lambda = 3.98\ a$ for T^* = 1.6, $\overline{\zeta}$ = 0.55.

There is a very small difference between the values of λ obtained for the two temperatures, and the difference decreases with an increase of $\overline{\zeta}$. Moreover, for $\overline{\zeta} > 0.3$ the dependence of λ on $\overline{\zeta}$ is weak, as in ref 4.

The values of the reduced temperature $T^* > T^*_\lambda$ for large $\overline{\zeta}$, however, are too high when compared to room temperature. A rough estimate of the reduced temperature that corresponds to the conditions for the LiTFSI salt in water at room temperature (T = 300 °C and ε = 80) is about 0.5. Assuming that the dielectric constant of bulk water is decreased proportionally to the ion concentration, we should consider $T^* < 0.5$.

4.2. Beyond the MF Approximation. In order to calculate the fluctuation contribution to the inverse correlation functions $\tilde{C}_{\alpha\beta}(k)$ in the Brazovskii-type approximation, we take into account the last term in eq 10 and solve the closed set of four equations for the unknowns k_0 and $\tilde{C}_{\alpha\beta}(k_0)$. The explicit forms of these equations are given in the Supporting Information. Once k_0 and $\tilde{C}_{\alpha\beta}(k_0)$ are determined, the inverse

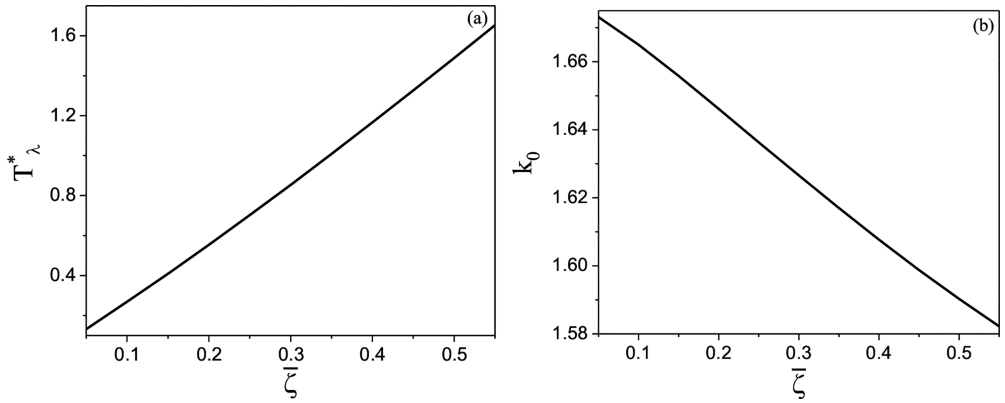

Figure 3. λ-line in $\overline{\zeta}$—T^* (panel a) and $\overline{\zeta}$—k_0 (panel b) coordinates for the model with δ = 0.5, ϵ^*_{++}=5.0, and ϵ^*_{--}=1.0. T^* and δ are defined in eq 5 and eq 7, respectively. $\overline{\zeta} = \overline{\zeta}_+ + \overline{\zeta}_-$ is the total volume fraction of ions, $\overline{\zeta}_\alpha = \pi\rho_\alpha\sigma_\alpha^3/6$, k_0 is in the a^{-1} units, $a = (\sigma_+ + \sigma_-)/2 \approx 0.4nm$.

https://doi.org/10.1021/acsomega.1c06013
ACS Omega 2022, 7, 6655−6664

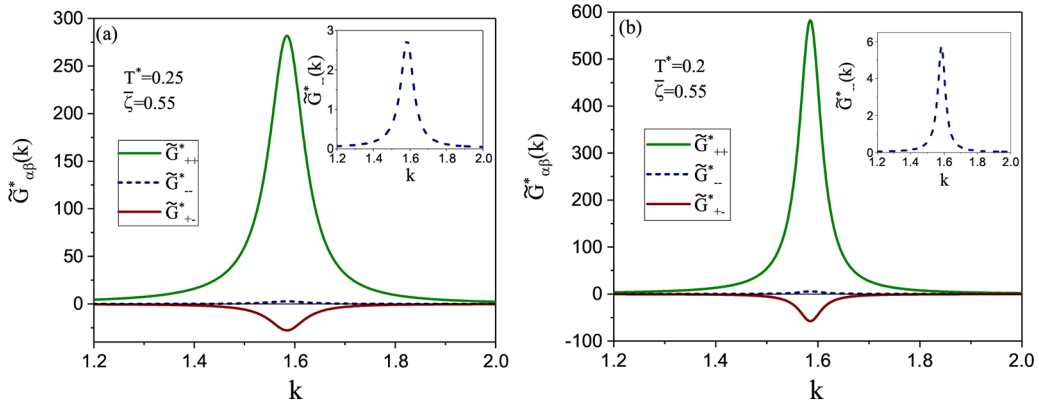

Figure 5. Correlation functions in Fourier representation with the effect of fluctuations taken into account for $T^* = 0.25$, $\bar{\zeta} = 0.55$ (panel a) and for $T^* = 0.2$, $\bar{\zeta} = 0.55$ (panel b). $\tilde{G}^*_{\alpha\beta} = \tilde{G}_{\alpha\beta}/\bar{\zeta}_\alpha\bar{\zeta}_\beta$, $\bar{\zeta}_\alpha = \pi\rho_\alpha\sigma_\alpha^3/6$, and the wavenumber k is in a^{-1} units with $a = (\sigma_+ + \sigma_-)/2$. The results are for the model with $\delta = 0.5$, $\epsilon^*_{++} = 5$, and $\epsilon^*_{++} = 1$. In the insets, we show sharp peaks of $\tilde{G}^*_{--}(k)$.

correlation functions $\tilde{C}_{\alpha\beta}(k)$ can be obtained from eqs 16 and 17.

From $\mathbf{G} = \mathbf{C}^{-1}$, one can calculate the correlation functions in Fourier representation. In Figure 5, we show the reduced correlation functions in Fourier representation $\tilde{G}^*_{\alpha\beta}(k) = \tilde{G}_{\alpha\beta}(k)/\bar{\zeta}_\alpha\bar{\zeta}_\beta$ for the fixed total volume fraction $\bar{\zeta} = 0.55$ and for two temperatures, $T^* = 0.25$ (panel a) and $T^* = 0.2$ (panel b). The three correlation functions $\tilde{G}^*_{\alpha\beta}(k)$ have sharp maxima for $k = k_0 \simeq 1.58$. For both temperatures, the height of the $\tilde{G}^*_{++}(k)$ maximum is about 100 times higher than the maximum of $\tilde{G}^*_{--}(k)$. It should be noted that the dependence of k_0 on T^* for the fixed $\bar{\zeta}$ is negligible, especially in the range $T^* = 0.2$–0.3 (see Table 1).

Table 1. Wave Number k_0, the Decay Length $\lambda_s = \alpha_0^{-1}$, and the Period of Oscillations $\lambda = 2\pi/\alpha_1$ of the Pair Correlation Functions $G_{\alpha\beta}(r)$ Depending on the Total Number Density $\bar{\zeta}$ for Fixed Values of Temperature T^*[a]

T^*	$\bar{\zeta}$	k_0	α_0	α_1	α_0^{-1}	$2\pi/\alpha_1$
0.4	0.45	1.597	0.225	1.613	4.444	3.895
0.4	0.5	1.591	0.163	1.599	6.151	3.930
0.4	0.55	1.582	0.119	1.587	8.424	3.959
0.3	0.45	1.602	0.124	1.607	8.042	3.910
0.3	0.5	1.593	0.088	1.595	11.426	3.939
0.3	0.55	1.584	0.063	1.585	15.796	3.964
0.25	0.45	1.605	0.084	1.607	11.852	3.911
0.25	0.5	1.594	0.059	1.595	16.920	3.939
0.25	0.55	1.584	0.043	1.585	23.411	3.964
0.2	0.45	1.607	0.053	1.608	19.016	3.907
0.2	0.5	1.595	0.037	1.596	27.191	3.937
0.2	0.55	1.585	0.027	1.585	37.610	3.963

[a] T^* is defined in eq 5, $\bar{\zeta} = \bar{\zeta}_+ + \bar{\zeta}_-$, $\bar{\zeta}_\alpha = \pi\rho_\alpha\sigma_\alpha^3/6$, and k_0, α_0, and α_1 are in a^{-1} units.

The reduced correlation functions in real-space representation, $G^*_{\alpha\beta}(r) = G_{\alpha\beta}(r)/\bar{\zeta}_\alpha\bar{\zeta}_\beta$, are obtained from the inverse Fourier transformation of $\tilde{G}^*_{\alpha\beta}(k)$. They are shown in Figure 6 for $T^* = 0.25$, $\bar{\zeta} = 0.55$ (panel a) and for $T^* = 0.2$, $\bar{\zeta} = 0.55$ (panel b). As seen, $G^*_{\alpha\beta}(r)$ shows exponentially damped oscillatory behavior, as described by eq 19. The period of damped oscillations is about $4a$. We study the asymptotic decay of the correlation functions $G_{\alpha\beta}(r)$ using the pole analysis. The results of this numerical analysis for $T^* = 0.2$, 0.25, 0.3, and 0.4 and for $\bar{\zeta} = 0.45$, 0.5, and 0.55 are summarized in Table 1. For the fixed volume fraction, the period $\lambda = 2\pi/\alpha_1$ coincides with $2\pi/k_0$ and is rather kept constant for $T^* \leq 0.3$. For the fixed temperature, λ is a weakly increasing function of ζ. It should be noted that the period of damped oscillations obtained with the effect of fluctuations taken into account is very close to the period obtained in MF for the higher temperature. By contrast, the decay length α_0^{-1} noticeably increases with an increase of $\bar{\zeta}$ for the fixed temperature, and this increase is more rapid for lower temperatures. In Figure 7, we present the decay length α_0^{-1} as a function of the total volume fraction of ions $\bar{\zeta}$ for fixed temperatures (panel a) and as a function of the Bjerrum length l_B for fixed volume fractions (panel b). One can observe that α_0^{-1} has a nearly linear dependence on the volume fraction for fixed T^*, with the slope decreasing with T^* and a nearly linear dependence on l_B for fixed $\bar{\zeta}$, with the slope increasing with $\bar{\zeta}$.

5. DISCUSSION

We have developed a highly simplified model for water-in-salt electrolytes and focused on the salt LiTFSI that was a subject of recent experiments.[3,4] In our model, the ions are treated as charged hard spheres with different diameters, and we assumed additional, water-mediated specific interactions between the ions of the same sign. We assumed that the solvent influences the distribution of the ions mainly by inducing effective interactions between them, and otherwise the solvent can be neglected. Next, we assumed that the detailed shape of the specific interactions is not important, as long as these interactions are strongly attractive but of a short range. We chose the Yukawa potentials for the specific interactions and adjusted the parameters to the LiTFSI by requiring the same scale of inhomogeneities as found experimentally. Importantly, the obtained sum of the Coulomb and specific interactions for both the anions and the cations is attractive at short distances and repulsive at large distances.

For this model, we calculated correlation functions for concentrated electrolytes for reduced temperatures close to room temperature, using our theory for binary mixtures with competing interactions.[38,39,43] There is no unique way of relating the volume fraction in the approximate theory to experimental molarity since we assumed spherical rather than ellipsoidal anions, and the values of the ion diameters in the theory are not precise. We considered volume fractions $0.45 \leq \bar{\zeta} \leq 0.55$ somewhat larger than in the experiment but of the same order of magnitude (the molarity 0.38–0.46 considered

https://doi.org/10.1021/acsomega.1c06013
ACS Omega 2022, 7, 6655−6664

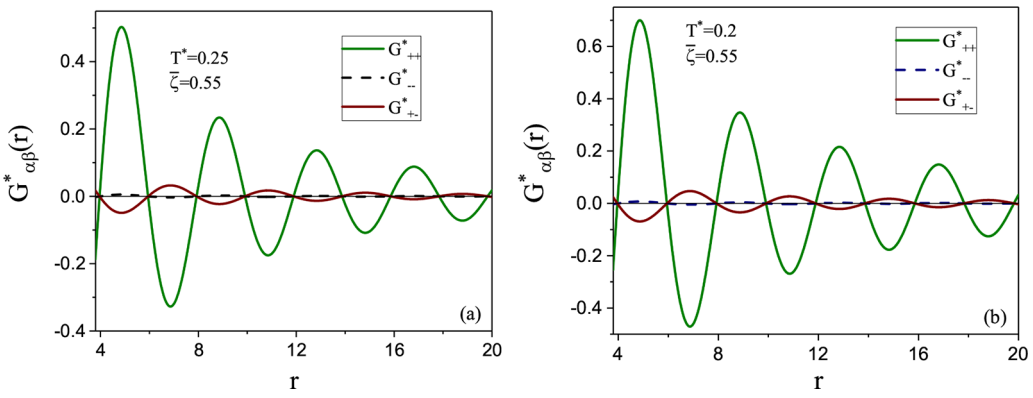

Figure 6. Correlation functions in real space with the effect of fluctuations taken into account for $\bar{\zeta} = 0.55$, $T^* = 0.25$ (panel a) and $T^* = 0.2$ (panel b). $G^*_{\alpha\beta} = G_{\alpha\beta}/\bar{\zeta}_\alpha\bar{\zeta}_\beta$, $\bar{\zeta}_\alpha = \pi\rho_\alpha\sigma_\alpha^3/6$, and r is in a units with $a = (\sigma_+ + \sigma_-)/2$. The results are for the model with $\delta = 0.5$, $\epsilon^*_{++} = 5$, and $\epsilon^*_{++} = 1$.

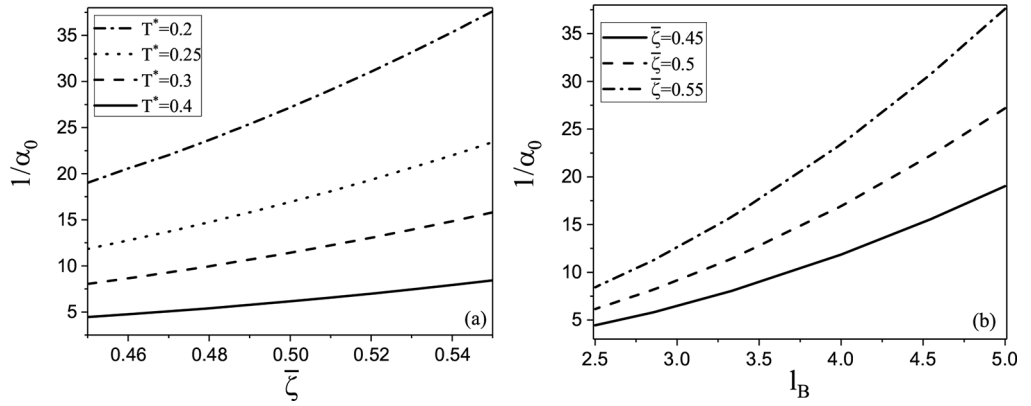

Figure 7. Decay length $\lambda_s = \alpha_0^{-1}$ of the correlation functions $G_{\alpha\beta}(r)$ as a function of the total volume fraction of ions $\bar{\zeta}$ for $T^* = 0.2$, 0.25, 0.3, and 0.4 (from the top to the bottom line) (panel a) and as a function of the Bjerrum length l_B for $\bar{\zeta} = 0.45$, 0.5, and 0.55 (from the bottom to the top line) (panel b). $1/\alpha_0$ and l_b are in a units, $a = (\sigma_+ + \sigma_-)/2 \approx 0.4$ nm. The results are for the model with $\delta = 0.5$, $\epsilon^*_{++} = 5$, and $\epsilon^*_{++} = 1$.

in ref 4 for spherical ions of our sizes gives $0.27 \le \bar{\zeta} \le 0.32$). We obtained exponentially damped oscillations for the correlation functions with the period $\lambda \approx 4$ in $a \approx 0.4$ nm units (in the experiment,[3,4] $\lambda \approx 1.4$ nm), very weakly depending on $\bar{\zeta}$ in the considered range of concentrations. In MF, λ decreases a bit. When the fluctuations are taken into account, λ increases with $\bar{\zeta}$. Interestingly, λ slightly decreases, increases, or does not change with increasing $\bar{\zeta}$, depending on the method of determining it in the experiment.[4]

We found that the decay length of the correlations, λ_s, increases almost linearly with $\bar{\zeta}$ for fixed reduced temperature T^*. It increases also with the Bjerrum length for temperatures of the order of room temperature. In particular, for the reduced temperature $T^* = 0.3$ (Bjerrum length $l_B = 3.3$ in $a \approx 0.4$ nm units), we obtain $\lambda_s \approx 3.2$–6 nm, and for $T^* = 0.2$ (Bjerrum length $l_B = 5$) we obtain $\lambda_s \approx 8$–15 nm for $\bar{\zeta} = 0.45$–0.55. These values are in semiquantitative agreement with the experimental decay lengths, $\lambda_s = 8.3$–11.5 nm, for the molarity 3.8–4.6 M ($\bar{\zeta} = 0.27$–0.32).

The approximate relation $\lambda_s \sim l_B\rho$ was discovered earlier for concentrated simple salts in water, ILs, and alkali halide solutions[12] and confirmed theoretically for the RPM (charged hard spheres with equal diameters and positive and negative charges of the same magnitude).[23] Our present results show that this relation is valid when ions with significantly different sizes interact with additional strong short-range potentials as well. It means that the dependence of λ_s on $l_B\rho$ does not depend on the length scale of inhomogeneity, at least in the range $2a - 4a$.

The very weak dependence of λ on $\bar{\zeta}$ and the semiquantitative agreement of the decay length with the experimental results indicate that the properties of the correlation functions do not depend sensitively on the details of the interactions. The ellipsoidal anions are approximated by the spherical ones; implicit solvent-inducing effective anion–anion and cation–cation interactions are assumed; and we neglected fluctuations of the dielectric constant induced by the concentration fluctuations. The dependence of the reduced temperature on $\bar{\zeta}$ (through the dependence of ϵ on $\bar{\zeta}$) was disregarded as well. The latter dependence for the rather narrow range of $\bar{\zeta}$ is not very strong, however. Finally, we rather arbitrarily assumed the shape of the specific interactions. With the above simplifications, we got semiquantitative agreement with experiments. It means that the above features are important only on the quantitative level.

We conclude that the key property determining the inhomogeneities on the mesoscopic length scale is the shape of the sum of the Coulomb and the solvent-induced specific interactions. In order to induce mesoscopic inhomogeneities, this sum should be attractive at short and repulsive at large distances, with the ranges and strengths of the attractive and repulsive parts determined by the properties of the ions and the solvent. If these anion–anion and cation–cation potentials have a negative minimum followed by a positive maximum, then layers of ions of the same sign and of the thickness

https://doi.org/10.1021/acsomega.1c06013
ACS Omega 2022, 7, 6655–6664

determined by the width and depth of the attractive well can be formed. We believe that this conclusion is not restricted to the particular case of the water-in-LiTFSI but applies to concentrated solutions of salts with significantly different solubility of cations and anions in charge-neutral solvents, such that the effective interactions have the form similar to the one shown in Figure 1. Hydrophilic cations and hydrophobic anions are present in the so-called "antagonistic salts", such as for example sodium tetraphenylborate ($NaBPh_4$). This salt induces strong mesoscopic inhomogenity on the length scale 10 nm in the D_2O/3-methylpyridine (3MP) mixture.[51−54] In concentrated solutions in water of this and some other antagonistic salts, mesoscopic charged regions correlated over large distances may be present. On the other hand, we expect that for a more complex anion structure than the structure of $TFSI^-$ the approximation of the anion shape by a sphere cannot be sufficient that it, in turn, can worsen the agreement between theoretical and experimental results. In particular, more elongated shape may lead to orientational ordering of the anions.

It is worth noting that our theory is formulated for the case when the valences of the cation and the anion are equal in magnitude but not necessarily equal to 1. Our theory can be extended to the case of unequal valences by changing the parameters in the Coulomb potentials 2−4. In principle, the theory could be extended to lithium salt/IL mixtures, but in a minimal model at least two types of cations and one type of anion, i.e., a three-component mixture, should be considered.

Finally, we have shown that the self-consistent theory with the local fluctuations of the volume fractions taken into account[38,39] can predict the structure with local inhomogeneities on a semiquantitative level.

There remains one unsolved problem—namely, the experimental disjoining pressure between crossed mica cylinders decays monotonically at large distances,[4] whereas our theory predicts the oscillatory decay. The same problem concerns simple salts and some other ILs modeled by the RPM.

■ ASSOCIATED CONTENT

Supporting Information

The Supporting Information is available free of charge at https://pubs.acs.org/doi/10.1021/acsomega.1c06013.

Interaction potentials in Fourier representation; free-energy density for a mixture of hard spheres with different diameters; inverse correlation functions in MF; and equations for the inverse correlation functions in Fourier representation when the fluctuations are taken into account (PDF)

■ AUTHOR INFORMATION

Corresponding Author

Oksana Patsahan − *Institute for Condensed Matter Physics of the National Academy of Sciences of Ukraine, Lviv 79011, Ukraine;* orcid.org/0000-0002-5839-3893; Email: oksana@icmp.lviv.ua

Author

Alina Ciach − *Institute of Physical Chemistry, Polish Academy of Sciences, 01-224 Warszawa, Poland;* orcid.org/0000-0002-5556-401X

Complete contact information is available at: https://pubs.acs.org/10.1021/acsomega.1c06013

Notes

The authors declare no competing financial interest.

■ ACKNOWLEDGMENTS

This project has received funding from the European Union Horizon 2020 research and innovation under the Marie Skłodowska-Curie grant agreement No. 734276 (CONIN). Additional funding was received from the Polish Ministry of Science and Higher Education for the implementation of the project No.734276 in the years 2017−2022.

■ REFERENCES

(1) Chen, M.; Feng, G.; Qiao, R. Water-in-salt electrolytes: An interfacial perspective. *Curr. Opin. Colloid Interface Sci.* **2020**, *47*, 99−110.

(2) Suo, L.; Borodin, O.; Gao, T.; Olguin, M.; Ho, J.; Fan, X.; Luo, C.; Wang, C.; Xu, K. "Water-in-salt" electrolyte enables high-voltage aqueous lithium-ion chemistries. *Science* **2015**, *350*, 938−943.

(3) Borodin, O.; et al. Liquid Structure with Nano-Heterogeneity Promotes Cationic Transport in Concentrated Electrolytes. *ACS Nano* **2017**, *11*, 10462−10471.

(4) Groves, T. S.; Perez-Martinez, C. S.; Lhermerout, R.; Perkin, S. Surface Forces and Structure in a Water-in-Salt Electrolyte. *J. Phys. Chem. Lett.* **2021**, *12*, 1702−1707.

(5) Gouverneur, M.; Schmidt, F.; Schönhoff, M. Negative effective Li transference numbers in Li salt/ionic liquid mixtures: does Li drift in the "Wrong" direction? *Phys. Chem. Chem. Phys.* **2018**, *20*, 7470−7478.

(6) Brinkkötter, M.; Giffin, G. A.; Moretti, A.; Jeong, S.; Passerini, S.; Schönhoff, M. Relevance of ion clusters for Li transport at elevated salt concentrations in [Pyr12O1][FTFSI] ionic liquid-based electrolytes. *Chem. Commun.* **2018**, *54*, 4278−4281.

(7) McEldrew, M.; Goodwin, Z. A. H.; Molinari, N.; Kozinsky, B.; Kornyshev, A. A.; Bazant, M. Z. Salt-in-ionic-liquid electrolytes: Ion network formation and negative effective charges of alkali metal cations. *J. Phys. Chem. B* **2021**, *125*, 13752.

(8) Molinari, N.; Mailoa, J. P.; Kozinsky, B. General Trend of a Negative Li Effective Charge in Ionic Liquid Electrolytes. *J. Phys. Chem. Lett.* **2019**, *10*, 2313−2319.

(9) Molinari, N.; Mailoa, J. P.; Craig, N.; Christensen, J.; Kozinsky, B. Transport anomalies emerging from strong correlation in ionic liquid electrolytes. *J. Power Sources* **2019**, *428*, 27−36.

(10) Gebbie, M. A.; Valtiner, M.; Banquy, X.; Fox, E. T.; Henderson, W. A.; Israelachvili, J. N. Ionic liquids behave as dilute electrolyte solutions. *Proc. Natl. Acad. Sci. U.S.A.* **2013**, *110*, 9674−9679.

(11) Smith, A. M.; Lee, A. A.; Perkin, S. The electrostatic screening lenght in concentrated electrolyte increases with concentration. *J. Phys. Chem. Lett.* **2016**, *7*, 2157−2163.

(12) Lee, A.; Perez-Martinez, C. S.; Smith, A. M.; Perkin, S. Scaling analysis of the screening length in concentrated electrolytes. *Phys. Rev. Lett.* **2017**, *119*, 026002.

(13) Kjellander, R. Focus Article: Oscillatory and long-range monotonic exponential decays of electrostatic interactions in ionic liquids and other electrolytes: The significance of dielectric permittivity and renormalized charges. *J. Chem. Phys.* **2018**, *148*, 193701.

(14) Kjellander, R. The intimate relationship between the dielectric response and the decay of intermolecular correlations and surface forces in electrolytes. *Soft Matter* **2019**, *15*, 5866−5895.

(15) Goodwin, Z. A.; Kornyshev, A. A. Underscreening, overscreening and double-layer capacitance. *Electrochem. Commun.* **2017**, *82*, 129−133.

(16) Ludwig, N. B.; Dasbiswas, K.; Talapin, D. V.; Vaikuntanathan, S. Describing screening in dense ionic fluids with a charge-frustrated Ising model. *J. Chem. Phys.* **2018**, *149*, 164505.

(17) Rotenberg, B.; Bernard, O.; Hansen, J.-P. Underscreening in ionic liquids: a first principles analysis. *J. Phys.: Condens. Matter* **2018**, *30*, 054005.
(18) Adar, R. M.; Safran, S. A.; Diamant, H.; Andelman, D. Screening length for finite-size ions in concentrated electrolytes. *Phys. Rev. E* **2019**, *100*, 042615.
(19) de Souza, J. P.; Goodwin, Z. A.; McEldrew, M.; Kornyshev, A. A.; Bazant, M. Z. Interfacial Layering in the Electric Double Layer of Ionic Liquids. *Phys. Rev. Lett.* **2020**, *125*, 116001.
(20) Outhwaite, C. W.; Bhuiyan, L. B. On the modified Poisson−Boltzmann closure for primitive model electrolytes at high concentration. *J. Chem. Phys.* **2021**, *155*, 014504.
(21) Coles, S. W.; Park, C.; Nikam, R.; Kanduč, M.; Dzubiella, J.; Rotenberg, B. Correlation Length in Concentrated Electrolytes: Insights from All-Atom Molecular Dynamics Simulations. *J. Phys. Chem. B* **2020**, *124*, 1778−1786.
(22) Zeman, J.; Kondrat, S.; Holm, C. Bulk ionic screening lengths from extremely large-scale molecular dynamics simulations. *Chem. Commun.* **2020**, *56*, 15635−15638.
(23) Ciach, A.; Patsahan, O. Correct scaling of the correlation length from a theory for concentrated electrolytes. *J. Phys.: Condens. Matter* **2021**, *33*, 37LT01.
(24) Stell, G. Criticality and phase transitions in ionic fluids. *J. Stat. Phys.* **1995**, *78*, 197−238.
(25) Fisher, M. E. The story of coulombic critiality. *J. Stat. Phys.* **1994**, *75*, 1−36.
(26) Leote de Carvalho, R.J.F.; Evans, R. The decay of correlations in ionic fluids. *Mol. Phys.* **1994**, *83*, 619−654.
(27) Ciach, A.; Góźdź, W. T.; Evans, R. Effect of a nearby charge-ordered phase on correlation functions in ionic systems. *J. Chem. Phys.* **2003**, *118*, 3702−3710.
(28) Patsahan, O.; Ciach, A. Correlation functions in an ionic liquid at coexistence with an ionic crystal: results of the Brazovskii-type field theory. *J. Phys.: Condens. Matter* **2007**, *19*, 236203.
(29) Kirkwood, J. G. Statistical mechanics of liquid solutions. *Chem. Rev.* **1936**, *19*, 275−307.
(30) Fedorov, M. V.; Kornyshev, A. A. Ionic liquid near a charged wall: Structure and capacitance of electrical double layer. *J. Phys. Chem. B* **2008**, *112*, 11868−11872.
(31) Fedorov, M. V.; Kornyshev, A. A. Ionic liquids at electrified interfaces. *Chem. Rev.* **2014**, *114*, 2978−3036.
(32) Ciach, A. Simple theory for oscillatory charge profile in ionic liquids near a charged wall. *J. Mol. Liq.* **2018**, *270*, 138−144.
(33) Ciach, A.; Stell, G. Effect of competition between Coulomb and dispersion forces on phase transitions in ionic systems. *J. Chem. Phys.* **2001**, *114*, 3617−3630.
(34) Ciach, A.; Góźdź, W. T.; Stell, G. Field theory for size- and charge asymmetric primitive model of ionic systems. Mean-field stability analysis and pretransitional effects. *Phys. Rev. E* **2007**, *75*, 051505.
(35) Patsahan, O. V.; Patsahan, T. M. Gas-liquid critical parameters of asymmetric models of ionic fluids. *Phys. Rev. E* **2010**, *81*, 031110.
(36) Patsahan, O. V.; Patsahan, T. M. Gas−liquid coexistence in asymmetric primitive models of ionic fluids. *J. Mol. Liq.* **2011**, *164*, 44−48.
(37) Patsahan, O.; Ciach, A. Spatial inhomogeneities in ionic liquids, charged proteins and charge stabilized colloids from collective variables theory. *Phys. Rev. E* **2012**, *86*, 031504.
(38) Ciach, A.; Patsahan, O.; Meyra, A. Effects of fluctuations on correlation functions in inhomogeneous mixtures. *Condens. Matter Phys.* **2020**, *23*, 23601.
(39) Patsahan, O.; Meyra, A.; Ciach, A. Correlation functions in mixtures with energetically favoured nearest neighbours of different kind: a size-asymmetric case. *Mol. Phys.* **2021**, *119*, 1820091.
(40) de Candia, A.; Del Gado, E.; Fierro, A.; Sator, N.; Tarzia, M.; Coniglio, A. Columnar and lamellar phases in attractive colloidal systems. *Phys. Rev. E* **2006**, *74*, No. 010403.
(41) Archer, A. J.; Wilding, N. B. Phase behavior of a fluid with competing attractive and repulsive interactions. *Phys. Rev. E* **2007**, *76*, 031501.
(42) Ciach, A.; Pękalski, J.; Góźdź, W. T. Origin of similarity of phase diagrams in amphiphilic and colloidal systems with competing interactions. *Soft Matter* **2013**, *9*, 6301−6308.
(43) Ciach, A. Mesoscopic theory for inhomogeneous mixtures. *Mol. Phys.* **2011**, *109*, 1101−1119.
(44) Mansoori, G. A.; Carnahan, N. F.; Starling, K. E.; Leland, T. W. Equilibrium thermodynamic properties of the mixture of hard spheres. *J. Chem. Phys.* **1971**, *54*, 1523−1525.
(45) Roth, R.; Evans, R.; Lang, A.; Kahl, G. Fundamental measure theory for hard-sphere mixtures revisited: the White Bear version. *J. Phys.: Condens. Matter* **2002**, *14*, 12063.
(46) Landau, L. D.; Lifshitz, E. M. *Statistical Physics*, 3rd ed.; Pergamon Press, 1989.
(47) Brazovskii, S. A. Phase transition of an isotropic system to a nonuniform state. *Sov. Phys. JETP* **1975**, *41*, 85−89.
(48) Ciach, A.; Patsahan, O. Effect of mesoscopic fluctuations on equation of state in cluster-forming systems. *Condens. Matter Phys.* **2012**, *15*, 23604.
(49) Patsahan, O.; Litniewski, M.; Ciach, A. Self-assembly in mixtures with competing interactions. *Soft Matter* **2021**, *17*, 2883−2899.
(50) Evans, R.; Leote de Carvalho, R. J. F.; Henderson, J. R.; Hoyle, D. C. Asymptotic decay of correlations in liquids and their mixtures. *J. Chem. Phys.* **1994**, *100*, 591−603.
(51) Sadakane, K.; Nagao, M.; Endo, H.; Seto, H. Membrane formation by preferential solvation of ions in mixture of water, 3-methylpyridine, and sodium tetraphenylborate. *J. Chem. Phys.* **2013**, *139*, 234905.
(52) Sadakane, K.; Onuki, A.; Nishida, K.; Koizumi, S.; Seto, H. Multilamellar Structures Induced by Hydrophilic and Hydrophobic Ions Added to a Binary Mixture of D_2O and 3-Methylpyridine. *Phys. Rev. Lett.* **2009**, *103*, 167803.
(53) Leys, J.; Subramanian, D.; Rodezno, E.; Hammouda, B.; Anisimov, M. A. Mesoscale phenomena in solutions of 3-methylpyridine, heavy water, and an antagonistic salt. *Soft Matter* **2013**, *9*, 9326.
(54) Pousaneh, F.; Ciach, A. The effect of antagonistic salt on a confined near-critical mixture. *Soft Matter* **2014**, *10*, 8188−8201.

https://doi.org/10.1021/acsomega.1c06013
ACS Omega 2022, 7, 6655−6664